Hindawi
Journal of Nanomaterials
Volume 2017, Article ID 2160278, 9 pages
https://doi.org/10.1155/2017/2160278

Research Article

Luminomagnetic Silica-Coated Heterodimers of Core/Shell FePt/Fe_3O_4 and CdSe Quantum Dots as Potential Biomedical Sensor

Caio Guilherme Secco de Souza,[1,2] João Batista Souza Jr.,[2] Watson Beck Jr.,[3] and Laudemir Carlos Varanda[2]

[1]*Departamento de Química, Universidade Federal de São Carlos (UFSCar), CP 676, 13565-905 São Carlos, SP, Brazil*
[2]*Instituto de Química de São Carlos, Universidade de São Paulo (USP), Colloidal Materials Group, CP 780, 13566-590 São Carlos, SP, Brazil*
[3]*Instituto Federal de Santa Catarina (IFSC), 89111-009 Gaspar, SC, Brazil*

Correspondence should be addressed to Laudemir Carlos Varanda; lvaranda@iqsc.usp.br

Received 15 February 2017; Revised 1 May 2017; Accepted 14 May 2017; Published 11 June 2017

Academic Editor: Miguel A. Garcia

We report the synthesis of a new multifunctional nanomaterial based on silica-coated FePt/Fe_3O_4-CdSe heteronanostructures, combining luminescent and magnetic properties in a promising bifunctional sensor for biomedical applications. Spherical Fe_3O_4-coated FePt (FePt/Fe_3O_4) superparamagnetic nanoparticles (10.8 ± 1.5 nm) with high saturation magnetization and controlled size and shape were obtained using thermal decomposition coupled with seed-mediated growth method. Luminescent property was added to the nanomaterial by using the FePt/Fe_3O_4 magnetic core as seed and growing the CdSe quantum dots (2.7 ± 0.6 nm) onto its surface in a heterodimer-like structure using the hot-injection approach. The FePt/Fe_3O_4-CdSe luminomagnetic heteronanostructures were coated with silica shell using the reverse-micelle microemulsion route to avoid solvent-quenching effects. After silica coating, the water-dispersible heteronanostructures showed a diameter of 25.3 ± 2 nm, high colloidal stability, magnetic saturation of around 11 emu g^{-1}, and photoluminescence in the blue-green region, as expected for potential bifunctional platform in biomedical applications. The saturation magnetization of heteronanostructures can be increased to 28 emu g^{-1} by annealing at 550°C due to the presence of the FePt phase.

1. Introduction

Recently, multifunctional nanomaterials with magnetic and luminescent properties have showed excellent features in potential biomedical applications in diagnosis and therapies, or as unique theranostic platform [1–3]. Among the different types of luminomagnetic nanomaterials, the heteronanostructures (HNS) show convenient response in biomedical applications, because its features provide properties related to two or more individual nanostructures in the unique nanomaterial [4–6]. Some applications of this theranostic platform include magnetic resonance imaging (MRI) [7], confocal and fluorescence imaging microscopies [4, 8] acting as contrast agents, cell separation and drug delivery [9, 10] as carriers, in both optic- and magnetohyperthermia [11, 12], in which the nanoparticles are the source of heat transfer, and photodynamic therapy by singlet oxygen generation [13]. Among various kinds of theranostic nanomaterials, those based on magnetic nanoparticles can achieve both diagnosis and therapy of cancer due to their magnetic property [14]. Hyperthermia treatment can be achieved using magnetic nanoparticles in the presence of an alternate magnetic field and the therapy success depends on the nanoparticles size, size distribution, magnetocrystalline anisotropy, and magnetization, among others [15]. Likewise, magnetic nanoparticles can also be used as T_2-weigthed contrast agents for MRI imaging [14]. Although different magnetic nanoparticles have already been tested for both in vivo and in vitro trials,

improving nanomaterials magnetization and synthesizing dual-mode imaging HNS based on MRI imaging and a secondary optical material could improve the theranostic performance [15]. Therefore, the possibility of tuning the photoluminescence of quantum dots can be added to the superparamagnetism property of magnetic nanomaterials to make a theranostic platform.

The HNS has been extensively discussed in the literature and its formation can be understood by the classical thermodynamics of crystals nucleation and growth theory [5, 6, 16]. According to the theory, the Gibbs energy to promote homogeneous nucleation in the reaction medium is higher than that required so that the heterogeneous nucleation takes place. The difference is associated with an increase in the surface energy for the homogeneous case promoted by the high interface tension between the monomers present in the reaction medium and the surface of freshly formed nuclei. In this way, the energy barrier to be overcome in the heterogeneous nucleation is much smaller than that for homogeneous nucleation. Therefore, HNS synthesis, such as core/shell or heterodimers, requires lower chemical potential to drive the monomers from reaction medium [5, 6, 16]. There are many strategies to prepare HNS, such as direct heterogeneous nucleation, reactions in liquid/liquid interfaces, seeded hot-injection approaches, and heteroconjugation using molecular surface engineering, among others [5, 16, 17]. Usually, the seed-mediated hot-injection synthesis has been used to obtain anisotropic HNS with controlled size and shape, which is essential to obtain a fast and narrow signal range response, besides a high signal-to-noise ratio [16, 17]. In this method, the precursors of the second nanomaterial of interest are injected at high temperature into the reaction medium containing the seeds of one primary nanostructure to promote its growing on the seed surface and generating the desired HNS. Size and shape of the second nanomaterial in the seed-mediated hot-injection synthesis can be achieved controlling the temperature, seeds to precursors ratio, reaction time, and the surfactants concentration in the reaction medium [18–20].

Colloidal stability and low nanoparticle toxicity are a requirement for biomedical applications [4, 8, 21, 22]. These features can be improved by adequate coating procedures used to functionalize the HNS surface with organic molecules as polyethylene glycol (PEG) [21, 22] and carboxymethyl dextran [23], polymers [24, 25], inorganic materials like silica [26, 27], and noble metals such as gold [28], among others [29, 30]. Silica coating is one of the most used procedures to functionalize nanostructures for biomedical application, either as single coating layer or as intermediate coating material for this purpose, because it prevents aggregation, improves colloidal stability, decreases toxicity, and increases the biocompatible characteristics of the nanomaterials [27, 31]. Kim and coworkers showed that silica-coated Fe_3O_4 nanoparticles had low toxicity and the Abraham group have also investigated silica-coated CdSe QDs showing the nontoxic behavior of these nanostructures [32, 33]. The main methods for silica coating are based on Stöber process [34] and, more recently, on the micelle-reverse microemulsion route [27]. Depending on the HNS surface features, that is, hydrophilic or hydrophobic behavior, the microemulsion route is preferable and provides more efficient control in the size, shape, and thickness of silica layer than Stöber method. Nowadays, the microemulsion route is the most used method to provide individual nanoparticle coating, because the formation of the silica coating is controlled by the micelles size.

Here, the method to obtain silica-coated FePt/Fe_3O_4-CdSe luminomagnetic HNS is described and its properties, focused on the biomedical application potential, are investigated. FePt/Fe_3O_4 magnetic nanoparticles (MNP), with high magnetization and superparamagnetic behavior, and CdSe quantum dots, with luminescent properties, are conjugated in a unique luminomagnetic platform nanomaterial. The magnetic core containing FePt nanoparticles coated with magnetite was chosen because it allows intensifying the saturation magnetization of the pure magnetite after annealing, as previously reported by our group [27, 35]. In addition, we use micelle-reverse microemulsion approach to provide the silica coating on HNS surface to enhance its colloidal stability in aqueous medium, decrease its toxicity, and minimize its luminescence quenching by solvent aiming potential biomedical applications.

2. Experimental Procedure

2.1. Materials. Iron(III) acetylacetonate ($Fe(acac)_3$, 99.0 %), platinum(II) acetylacetonate ($Pt(acac)_2$, 97.0%), cadmium(II) acetylacetonate ($Cd(acac)_2$, 99.9%), selenium dioxide (SeO_2, 99%), dibenzyl ether (99.0%), octyl ether (97.0%), oleic acid (90.0%), oleylamine (70.0%), hexane (99.0%), cyclohexane (99.0%), ethanol (99.5%), methanol (99.8%), isopropyl alcohol (99,7%), ammonium hydroxide (30 % in water), tetraethyl orthosilicate (98%), and Igepal CO-520® (average M_n 441) were purchased from Sigma Aldrich and used without further purifications.

2.2. FePt/Fe_3O_4 Magnetic Nanoparticles Core Synthesis. FePt/Fe_3O_4 magnetic nanoparticles were synthesized by the modified polyol process combined with the seed-mediated growth method based on early reported procedure as follows [27, 35]: $Pt(acac)_2$ (0.6 mmol), $Fe(acac)_3$ (0.73 mmol), and 1,2-hexadecanediol (1.5 mmol) were mixed in a three-necked round-bottom flask containing dibenzyl ether (20.0 mL). Under nitrogen blanket and stirring, the mixture was heated ($3^\circ C\,min^{-1}$) at 100°C and oleic acid (0.8 mmol) and oleylamine (0.8 mmol) was injected via syringe. The system was heated ($5.0^\circ C\,min^{-1}$) to reflux (298°C) for 30 min and then cooled to room temperature. When the system reached the room temperature, FePt nanoparticles were purified 3 times by hexane and ethanol addition and centrifuging. After that, purified FePt nanoparticles (250.0 mg), $Fe(acac)_3$ (5.0 mmol), 1,2-hexadecanediol (15.0 mmol), oleic acid (5.0 mmol), and oleylamine (5.0 mmol) were mixed in a three-necked round-bottom flask containing dibenzyl ether (20.0 mL) under nitrogen blanket. The temperature of the system was increased ($5.0^\circ C\,min^{-1}$) and kept at 100°C for 20 min and then raised ($10.0^\circ C\,min^{-1}$) to 200°C for 1.0 h and finally was

heated (10.0°C min^{-1}) to reflux (298.0°C) for 30 min before cooling down to room temperature. The resulting black suspension was purified by hexane and ethanol addition and centrifuging. Then, the magnetic nanoparticles were oven dried for 2 hours at 100°C and then heat treated at 550°C for 30 minutes in a tubular furnace (Thermolyne F79400) under nitrogen containing 5% of hydrogen atmosphere. The annealed Fe_3O_4-coated FePt nanoparticles were dispersed into hexane and stored.

2.3. Synthesis of FePt/Fe_3O_4-CdSe Luminomagnetic HNS. This synthetic route was performed using the seed-mediated hot-injection method with some modifications [36]. In a typical reaction, using a three-necked round-bottom flask, FePt/Fe_3O_4 magnetic nanoparticles (10 mg), cadmium acetylacetonate (0.1 mmol), oleic acid (200 μL), and oleylamine (200 μL) in octyl ether (20 mL) were added under room temperature and stirring. After that, the system was heated (5°C min^{-1}) to 160°C under nitrogen atmosphere and then injected 50 μL of selenium dioxide in methanol (2 mol L^{-1}) via syringe. After injection, the system was kept 1 min under stirring at high temperature and rapid cooled in a bath ice until reaching room temperature to prevent undesired growth of the CdSe quantum dots. The final product was washed three times with hexane/ethanol mixture and centrifuged to remove the supernatant with impurities. After that, the product was washed 5 times with hexane/ethanol mixture and the heteronanostructures were collected by magnetic separation and the FePt/Fe_3O_4-CdSe HNS were dispersed into cyclohexane and stored.

2.4. Silica Coating of Luminomagnetic HNS. The reverse-micelle microemulsion route was used to obtain silica coating onto individual HNS [27]. Firstly, Igepal CO-520 (700 μL) was added in cyclohexane (10 mL). The system was stirred for 15 min at room temperature, using a tube rotator. Then, 4.0 mL of FePt/Fe_3O_4-CdSe heteronanostructures dispersed in cyclohexane (2.5 mg mL^{-1}) was added to reaction system, and it was kept under stirring around 15 min. After this time, 110 μL of ammonium hydroxide ($NH_4OH_{(aq.)}$, 30%) was added and system continuously stirred for 15 min. Finally, 130 μL of tetraethyl orthosilicate (TEOS) was added and stirred at room temperature for 24 h, washed three times with methanol and two times with isopropanol, and separated by centrifugation to remove the supernatant with impurities. The silica-coated FePt/Fe_3O_4-CdSe heteronanostructures were dispersed in water and stored.

2.5. Characterization. Transmission electron microscopy (TEM) was performed in both the Philips CM200 and JEM-2100 JEOL microscopes operating at 200 kV. The samples were prepared by dropping dilute particle dispersion onto a carbon-coated copper grid, and the solvent slowly evaporated at room temperature. Average particle size was statistically determined by counting around 200 nanoparticles. X-ray powder diffraction was performed by a Bruker D8 Advance using Cu-Kα radiation (λ = 1.5406 Å). The photoluminescence spectra were obtained at room temperature in a FLUOROLOG SPEX 212L with a 450 W xenon continuous lamp equipped with a Hamamatsu R928 photomultiplier. The magnetic measurements were performed by conventional vibration sample magnetometer (VSM) and by Magnetic Property Measurement System (MPMS®3) combined with a SQUID sensor (Quantum Design©, in the laboratory SQUID-UFSCAR-QD-MPMS3, FAPESP 09/054083-2). The magnetic hysteresis loops were performed at room temperature with fields up to 2 T.

3. Results and Discussion

The polyol process coupled to seed-mediated growth was used to synthesize FePt/Fe_3O_4 magnetic nanoparticles in a core/shell nanostructure. The first step of synthesis involves the modified polyol process to obtain spherical FePt nanoparticles. This method is widely used in the literature to synthesize nanoparticles with controlled shape, size, and chemical composition, as well as narrow size distribution, that is, monodisperse systems [37, 38]. As-synthesized FePt nanoparticles presented average diameter and standard deviation ($\overline{x}$ ± SD) of 4.0 ± 0.2 nm in a monodisperse system measured by TEM analysis (D_{TEM}), average composition of $Fe_{55}Pt_{45}$, and face-centered cubic (fcc) crystallographic phase, as in a good agreement with the previously reported work [35]. After the magnetite coating, the nanoparticles maintained the spheroidal shape and the average particle diameter was increased to D_{TEM} = 10.8 ± 1.5 nm, which corresponds to a slightly large particle size distribution with polydispersity degree (SD/$\overline{x}$) around 0.14 (Figure 1(a)).

This result suggests that the magnetite layer with around 3.5 nm in thickness was formed onto the FePt nanoparticles. Previous reported work by our group has shown that the composition $Fe_{55}Pt_{45}$ favors the formation of the face-centered tetragonal (fct) phase of FePt during annealing. The tetragonal phase has a high uniaxial anisotropic constant (hard magnet), modifying the interactions and magnetic couplings acting on the nanoparticle [27, 35, 37]. According to previous results [35], during the coating procedure, iron atoms diffusional process takes place leading to a chemical composition gradient from Pt-rich FePt phase in the core, an intermediate Fe-rich FePt soft magnetic phase, and an outer ferrimagnetic magnetite phase from core to the nanoparticle surface. This composition gradient increases the saturation magnetization of the coated particle when compared to the pure magnetite, besides also contributing to increasing the chemical stability against the oxidation processes [35].

The methodology of synthesis based on hot injection was used to promote the formation of quantum dots. In this methodology, rapid and intense nucleation formation occurs due to the hot temperature of the reaction medium. According to the classical thermodynamic theory of nucleation and growth, the high surface energy of fresh nuclei favors heterogeneous nucleation onto the surface of the magnetic seeds present in the medium, to the detriment of homogeneous nucleation. As many nuclei are formed, those that are not found heterocoagulated on the magnetic nanoparticles present higher surface energy and tend to dissolve [6]. Thus, the growth of quantum dots occurs preferentially in the heterocoagulated nuclei leading to the formation of heteronanostructures.

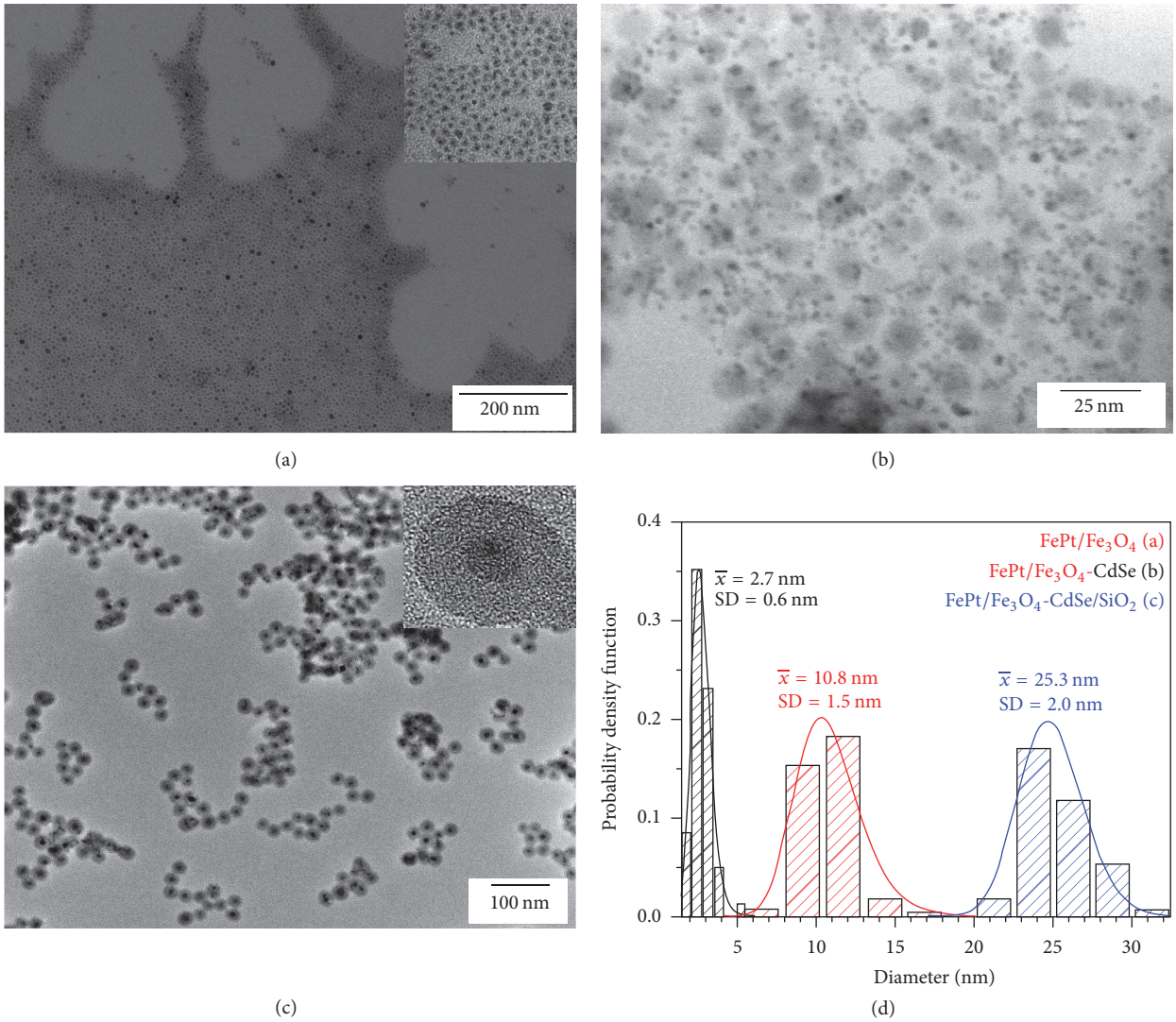

Figure 1: TEM images of the obtained nanoparticles in each synthesis route: (a) as-synthesized FePt/Fe_3O_4, (b) FePt/Fe_3O_4-CdSe HNS after magnetic separation, (c) silica-coated FePt/Fe_3O_4-CdSe HNS, and (d) size distribution histogram of the silica-coated HNS. Inset in (a) shows details of the iron oxide layer onto the metallic FePt core and in (c) shows an individual silica-coated HNS particle with distinguished contrast among the different phases.

The FePt/Fe_3O_4-CdSe HNS TEM image is presented in Figure 1(b) showing the CdSe nanoparticles (dark contrast) with average diameter of 2.7 ± 0.6 nm uniformly distributed on the magnetic nanoparticle surface. The heteronanostructured materials showed hydrophobic behavior, due to the presence of oleic acid and oleylamine on its surface. To provide hydrophilic surface and colloidal stability in aqueous solution, HNS were coated with silica shell using reverse-micelle microemulsion route. Typically, silica coating based on the Stöber method is performed on particles having a hydrophilic surface in polar solvents such as water or alcohol [34, 39]. Regarding the hydrophobic character of the as-synthesized HNS, the traditional Stöber method could not be used, and a variant procedure involving a reverse-micelle system was employed. The reverse-micelle microemulsion route allows dispersing the hydrophobic HNS into the micelle, which was also used as a reactor to limit the silica growth layer on individual HNS. After silica coating to provide water-dispersible system, silica-coated FePt/Fe_3O_4-CdSe HNS (Figure 1(c)) show average diameter of D_{TEM} = 25.3 ± 2 nm with controlled size and morphology. The inset in Figure 1(c) shows an individual silica-coated HNS with silica layer thickness around 7 nm homogenously distributed on the surface of the HNS that present two different contrasts assigned to FePt/Fe_3O_4 (intermediate) and CdSe (dark) nanoparticles, respectively. According to histogram of size distribution of silica-coated HNS in Figure 1(d), the polydispersity degree was 0.08, which shows controlled monodisperse system with narrow size distribution. Although, specifically in this work, in vitro cytotoxicity assays with silica-coated heteronanostructures were not performed yet, there are many studies in the literature that have demonstrated the efficiency of the

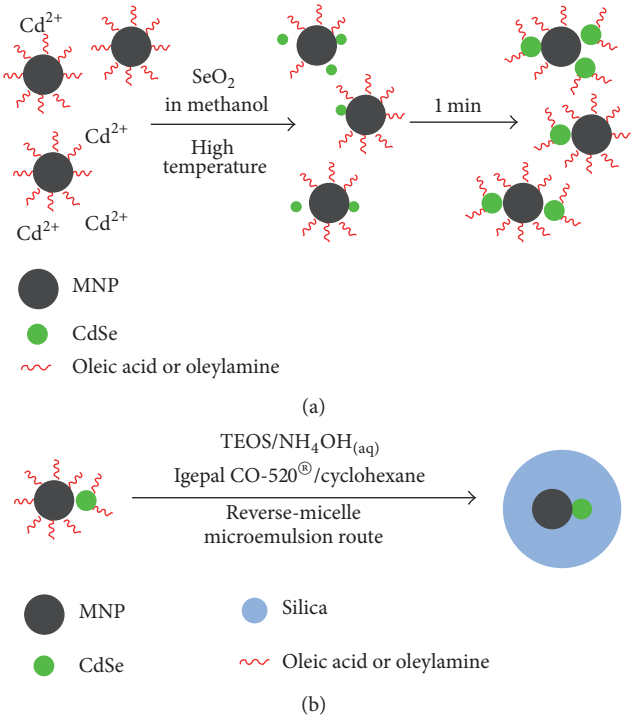

FIGURE 2: Schematic representation of the synthesis procedure used to produce (a) FePt/Fe_3O_4-CdSe HNS by modified polyol process combined with seed-mediated growth method and (b) silica-coated FePt/Fe_3O_4-CdSe HNS by reverse-micelle microemulsion route.

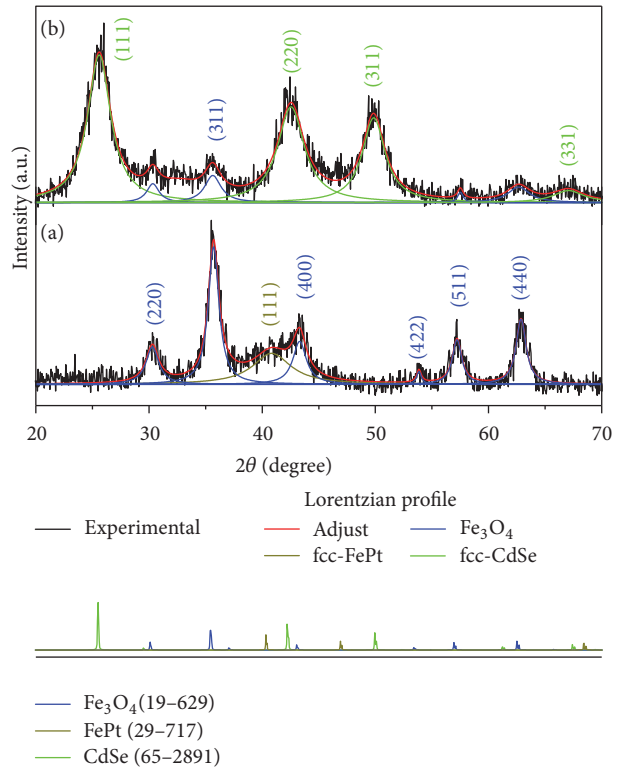

FIGURE 3: XRD patterns and the respective JCPDS standards (numbers in parentheses) of the (a) magnetic nanoparticles core (FePt/Fe_3O_4) and (b) the HNS after the CdSe formation onto the magnetic core surface (FePt/Fe_3O_4-CdSe) before annealing. Lines correspond to the adjustment of shape profile fitted from Lorentz equation according to the different phases present in the sample, identified by colors.

silica coating, reducing cytotoxicity, increasing the biocompatibility and the circulation time for all nanoparticle studied in vitro and in vivo systems [32, 33].

The representative scheme of the formation of HNS with the growth of CdSe on magnetic nanoparticle surface and subsequently silica coating on HNS previously obtained is showed in Figure 2.

Luminomagnetic dimers were obtained through heterogeneous nucleation of CdSe into magnetic nanoparticles surface using the seed-mediated method. Hydrophobic magnetic nanoparticles dispersed in dioctyl ether as solvent in the presence of cadmium precursor were heated and SeO_2 was injected at high temperature to achieve supersaturation. After SeO_2 solution injection, a fast heteronucleation of CdSe takes place and quantum dots grow on the magnetic nanoparticle surface. After one minute, the temperature of the reaction mixture was rapidly decreased to stop CdSe growth and obtain FePt/Fe_3O_4-CdSe luminomagnetic HNS. The CdSe size and, consequently, the fluorescence emission can be tuned using different growth time. HNS products were obtained and magnetically isolated to guarantee the formation of FePt/Fe_3O_4-CdSe dimers. As Fe_3O_4 has inverse spinel structure and CdSe has cubic zinc blend structure, the lattice mismatch for the [111] direction (27.7%) is high to support core/shell formation [6, 16]. Then, the growth of CdSe into magnetite surface would be preferentially in a facet with nearest crystallographic compatibility, generating dimers nanostructures [16].

Figure 3 shows the X-rays diffraction (XRD) results of the magnetic nanoparticle core before and after CdSe heterocoagulation by seed-mediated growth method and before the thermal treatment used to anneal the magnetic core. The diffraction patterns analyses were performed using the shape profile module with the Lorentz function to fit the XRD profiles by the TOPAS 4.1 software. The results shown in Figure 3 with the Lorentzian adjustment are only comparative, since the presence of different structures in the same nanoparticle, especially of the magnetite coating layer, did not allow applying a structural Rietveld refinement procedure. In Figure 3, XRD patterns of the magnetic nanoparticle core infer the presence of fcc-FePt phase identified by broadened and with low intensity reflections centered in 40.9° in 2θ degree, assigned to (111) diffraction planes. The low intensity of the fcc-FePt phase reflections can be explained by the magnetite coating layer thickness, which reduces the penetration of the X-ray beam to reach the metallic core. The average crystallite size (d_{XRD}) calculated by Scherrer equation [40] using the full width at half maximum (FWHM) of the (111) fcc-FePt reflection was found around 2.2 ± 0.3 nm. The comparison with the D_{TEM} value of the 4.0 nm suggests that the FePt nanoparticles were composed of 1.5–2.0 nanocrystals, as expected for as-synthesized chemical

disordered fcc phase [41]. The majority of reflections patterns in this sample are attributed to the spinel phase of the Fe_3O_4 with peaks centered at 30.3°, 35.7°, 43.3°, 53.8°, 57.2°, and 62.9° in 2θ degree related to (220), (311), (400), (422), (511), and (440) diffraction planes, respectively. The crystallite size evaluation was not used for the magnetite phase because it can lead to mismatch results due to the layered structure and, mainly, to the diffusion processes occurring between the platinum (core) and iron (core and coating) atoms during the synthesis at high temperature.

In the XRD patterns after the CdSe synthesized onto the magnetic core nanoparticle surface, it is possible to identify three intense peaks from CdSe phase that were centered at 25.6°, 42.5°, and 49.8° in 2θ degree assigned, respectively, to (111), (220), and (311) planes, besides a low intensity reflection at 67.1° related to (331) planes. This result confirms the presence of the CdSe luminescent quantum dots in the cubic phase (fcc), called sphalerite or zinc blende phase, differently to the wurtzite phase observed when the widely known as TOPO-TOP method [36, 42, 43] is used to produce CdSe nanoparticles with controlled size and shape. The FWHM of the reflection from (111) planes was used to calculate the average crystallite size of the quantum dots resulting in a value of the 3.0 ± 0.1 nm. The calculated value is in a good agreement with the D_{TEM} = 2.7 ± 0.6 nm suggesting a single crystal system of the CdSe. The XRD results of the HNS also show the more intensity reflections of the magnetite phase and the absence of the FePt reflections, probably, due to XRD beam penetrations. The comparative more intensity reflections from CdSe phase can be explained by the high crystallinity phase observed for the quantum dots, which results in a higher total number of coherent scattering domains.

The magnetic measurements for the $FePt/Fe_3O_4$ magnetic nanoparticle core (black line), $FePt/Fe_3O_4$-CdSe HNS (red line), and silica-coated HNS (blue line) are showed in Figure 4. The results presented in the hysteresis loops (Figure 4) consider the total sample mass, without correction related to the effective mass presented only by the magnetic core. The superparamagnetic behavior is observed in all cases, inferring that the main magnetic property remains after the CdSe quantum dots heterocoagulation, as well as also after the silica coating procedure. Superparamagnetic behavior is essential to be applied a nanoparticulate magnetic systems in biomedicine. Magnetic interparticles coupling may lead to the formation of aggregates large enough to cause capillary embolism. The superparamagnetic behavior results in nanoparticulate system that does not present intrinsic magnetic moment in the absence of external magnetic field [44]. Thus, the superparamagnetic nanoparticles are magnetized in the presence of an external field and, immediately after its removal, the response is lost, resulting in a nonaggregated magnetic system. The superparamagnetic behavior can be observed by low coercivity values showed in Figure 4 inset. The saturation magnetization for $FePt/Fe_3O_4$ magnetic nanoparticle, $FePt/Fe_3O_4$-CdSe HNS, and silica-coated HNS is 46.8, 24.1, and 11.1 emu g^{-1}, respectively. As mentioned, the decrease of saturation magnetization values is attributed to the nonmagnetic materials addition. After the heat treatment,

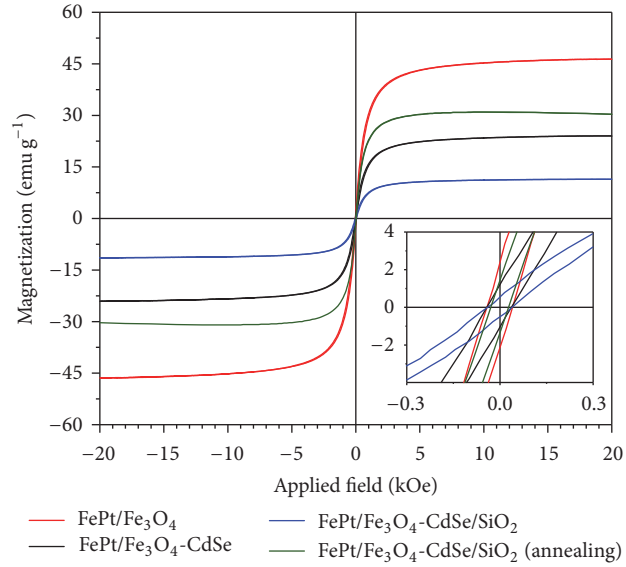

Figure 4: Hysteresis loops at room temperature for $FePt/Fe_3O_4$ magnetic nanoparticles core (red line), $FePt/Fe_3O_4$-CdSe HNS (black line), and $FePt/Fe_3O_4$-CdSe/SiO_2 HNS before (blue line) and after (green line) thermal annealing without correction of the nonmagnetic materials contribution.

the sample silica-coated HNS presents increase in the saturation magnetization value, from 11.1 emu g^{-1} to 28.2 emu g^{-1}, without meaningful change in the superparamagnetic behavior, as expected after the annealing process [35]. In a general way, however, the saturation magnetization values of both annealed and nonannealed HNS are high enough to allow the application as theranostic system in biomedical applications [1, 15].

UV-Vis and emission spectra (λ_{exc} = 400 nm) for $FePt/Fe_3O_4$-CdSe HNS and CdSe quantum dots were showed in Figure 5. CdSe quantum dots were produced in the absence of magnetic nanoparticles to compare with the optical properties of both systems. The first three excitons can be seen on the UV-Vis spectra of CdSe quantum dots showing the formation of homogenous particles [43, 45]. The first excitonic band located at 516.7 nm, $1S(e) - 1S_{3/2}(h)$ transition, indicated that the mean quantum dots diameter is ~2.64 nm using Jasieniak and coworkers equation [46], and a band gap energy value about 2.42 eV was obtained using Karel Čapek and coworkers equation for zinc blend CdSe [47]. The emission spectra show an intense photoluminescence around 534 nm (2.32 eV) with quantum yield up to 5% compared to Rhodamine 6G [46, 48].

$FePt/Fe_3O_4$-CdSe HNS showed a broad absorption band for the $1S(e) - 1S_{3/2}(h)$ transition at 512 nm, which gives a mean diameter of 2.58 nm and a band gap of 2.44 eV. The heterogeneous nucleation and growth process of CdSe into $FePt/Fe_3O_4$ surface led to slightly larger size distribution, as seen by the higher FWHM for the heteronanostructures compared to CdSe quantum dots. Photoluminescence spectrum (λ_{exc} = 400 nm) of the HNS showed the presence of the similar emission bands, related to the absorption band

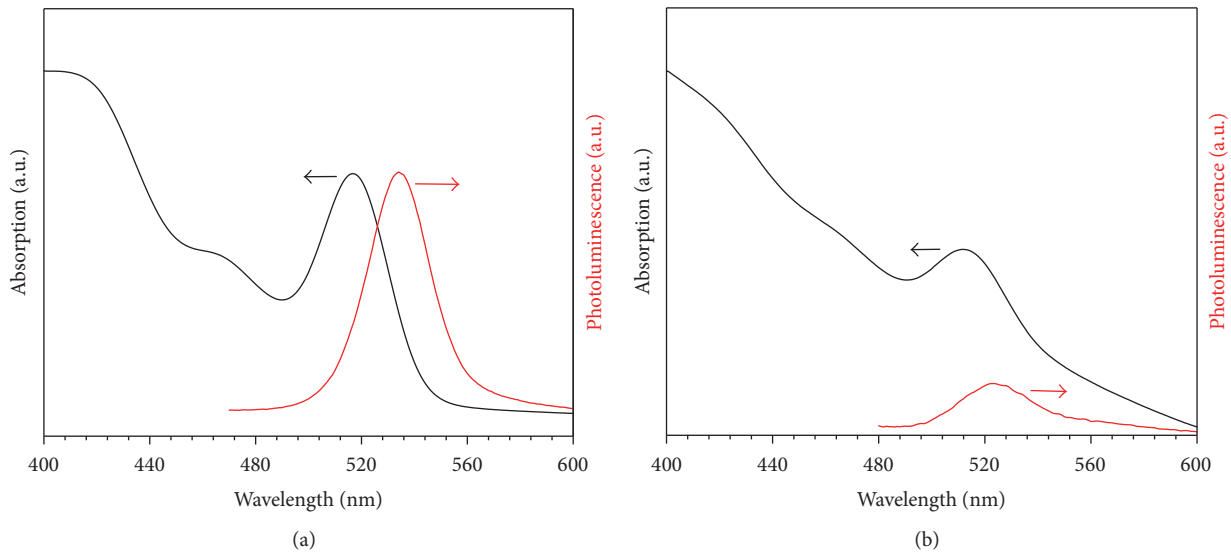

Figure 5: UV-Vis (black) and photoluminescence spectra (red) for (a) CdSe quantum dots and (b) FePt-Fe_3O_4-CdSe HNS.

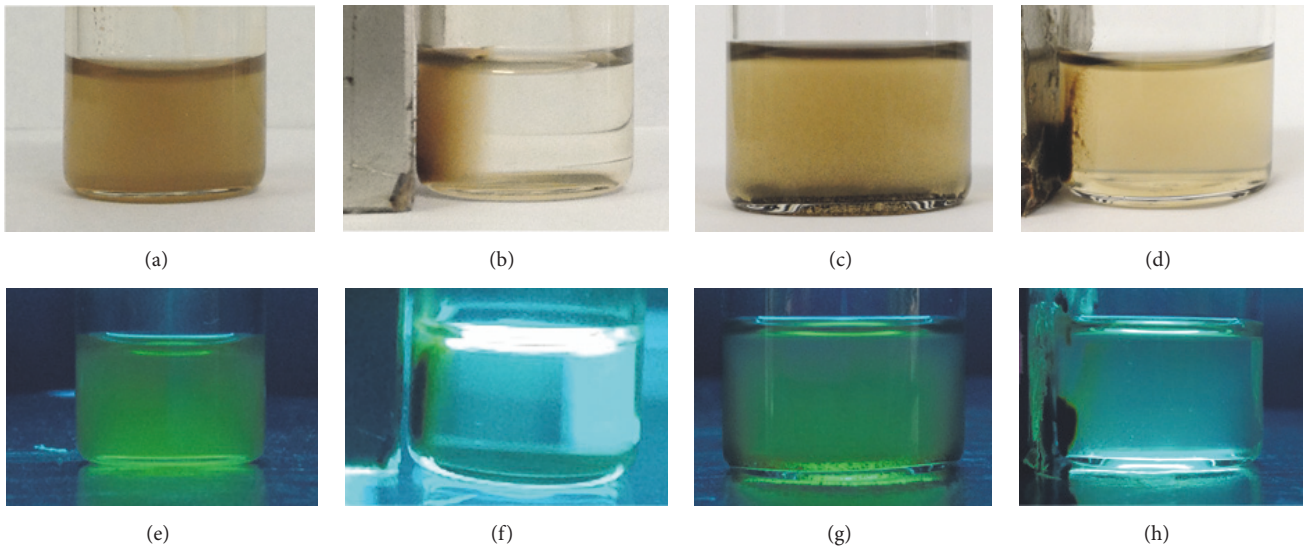

Figure 6: Images of FePt-Fe_3O_4-CdSe HNS under white light without (a and c) and in the presence of a magnet (b and d) and under UV light without (e–g) and in the presence of a magnet (f–h). Both sets of images are for nonannealed samples.

near 512 nm with maximum emission at 522 nm, but with lower intensity and being broadened in comparison with the pure CdSe quantum dots. Quantum yields of FePt/Fe_3O_4-CdSe HNS were estimated as below 1%, smaller than CdSe quantum dots. The formation of heterostructures of quantum dots is expected to have lower emission efficiency due to the presence of the crystal interface, which can possibly lead to dangling bonds or surface defects on CdSe. However, as shown here, FePt/Fe_3O_4-CdSe HNS have both properties desired for biomedical applications, superparamagnetism of the core/shell FePt/Fe_3O_4 particles and photoluminescence of CdSe quantum dots, as displayed on Figure 6.

Figure 6 shows the images for the samples of hydrophobic HNS (dispersed in hexane) and HNS after silica coating (dispersed in water), before and after applied magnetic field and UV light. This figure shows the samples of hydrophobic HNS ((a) and (b)) and silica-coated HNS ((c) and (d)) before and after applied magnetic field, respectively; and, in the presence of UV light, the samples of hydrophobic HNS ((e) and (f)) and silica-coated HNS ((g) and (h)) are also showed before and after applied magnetic field.

FePt/Fe_3O_4-CdSe HNS and silica-coated HNS images in the presence and absence of a magnetic field and UV excitation light are shown on Figure 6. FePt/Fe_3O_4-CdSe HNS showed high colloidal stability in hexane and all heteronanostructures can be separated from solution using a magnet. Similarly, after the formation of the silica shell, silica-coated HNS showed good colloidal stability in water

with a formation of some aggregates after few hours. Most of nanoparticles are immediately separated from solution using a magnet, and long time is necessary to separate all particles indicating superior colloidal stability of this system in water. FePt/Fe_3O_4-CdSe HNS showed a green emission in the presence of the UV excitation light due to the presence of the emission band around 522 nm. It was possible to visualize that in the presence of the magnetic field the emission is only seen in the precipitate on the edge of the flask, demonstrating that the magnetism from FePt/Fe_3O_4 and the photoluminescence from CdSe is structurally linked on both FePt/Fe_3O_4-CdSe HNS and silica-coated HNS.

4. Conclusions

The hot-injection method showed to be suitable to synthesize FePt/Fe_3O_4-CdSe luminomagnetic HNS with controlled size and shape, narrow size distribution, superparamagnetic behavior, high saturation magnetization, and photoluminescence after the formation of the HNS between FePt/Fe_3O_4 MNP and CdSe QD. The silica coating process using reverse-micelle microemulsion route provided silica-coated FePt/Fe_3O_4-CdSe luminomagnetic HNS with size and polydispersity degree around 25 nm and 8.0%, respectively. The saturation magnetization of silica-coated HNS was around 11 emu g^{-1} with superparamagnetic behavior, but the saturation magnetization can be increased to 28 emu g^{-1} by annealing at 550°C in nitrogen containing 5% of hydrogen atmosphere. The photoluminescence, with excitation at 400 nm, showed the emission band centered at 512 nm in the green-blue visible region. The integrated luminomagnetic properties and the suitable colloidal stability describe the potential biological applications of these heteronanostructures as theranostic materials.

Conflicts of Interest

The authors declare that they have no conflicts of interest.

Acknowledgments

This work was supported by Fundação de Amparo à Pesquisa do Estado de São Paulo (FAPESP) (no. 2007/07919-9; no. 2013/01284-2; no. 2012/02093-3) and Conselho Nacional de Desenvolvimento Científico e Tecnológico (CNPq) (no. 577166/2008-5) Brazilian agencies.

References

[1] O. Chen, L. Riedemann, F. Etoc et al., "Magneto-fluorescent core-shell supernanoparticles," *Nature Communications*, vol. 5, p. 5093, 2014.

[2] R. Kas, E. Sevinc, U. Topal, and H. Y. Acar, "A universal method for the preparation of magnetic and luminescent hybrid nanoparticles," *Journal of Physical Chemistry C*, vol. 114, no. 17, pp. 7758–7766, 2010.

[3] F. Erogbogbo, K.-T. Yong, R. Hu et al., "Biocompatible magnetofluorescent probes: luminescent silicon quantum dots coupled with superparamagnetic iron(III) oxide," *ACS Nano*, vol. 4, no. 9, pp. 5131–5138, 2010.

[4] R. Costi, A. E. Saunders, and U. Banin, "Colloidal hybrid nanostructures: a new type of functional materials," *Angewandte Chemie International Edition*, vol. 49, no. 29, pp. 4878–4897, 2010.

[5] P. D. Cozzoli, T. Pellegrino, and L. Manna, "Synthesis, properties and perspectives of hybrid nanocrystal structures," *Chemical Society Reviews*, vol. 35, no. 11, pp. 1195–1208, 2006.

[6] C. de Mello Donega, "Synthesis and properties of colloidal heteronanocrystals," *Chemical Society Reviews*, vol. 40, no. 3, pp. 1512–1546, 2011.

[7] B. H. Kim, N. Lee, H. Kim et al., "Large-scale synthesis of uniform and extremely small-sized iron oxide nanoparticles for high-resolution T_1 magnetic resonance imaging contrast agents," *Journal of the American Chemical Society*, vol. 133, no. 32, pp. 12624–12631, 2011.

[8] C. Barrera, A. Herrera, Y. Zayas, and C. Rinaldi, "Surface modification of magnetite nanoparticles for biomedical applications," *Journal of Magnetism and Magnetic Materials*, vol. 321, no. 10, pp. 1397–1399, 2009.

[9] J. Kim, J. E. Lee, J. Lee et al., "Magnetic fluorescent delivery vehicle using uniform mesoporous silica spheres embedded with monodisperse magnetic and semiconductor nanocrystals," *Journal of the American Chemical Society*, vol. 128, no. 3, pp. 688-689, 2006.

[10] C. Sun, J. S. H. Lee, and M. Zhang, "Magnetic nanoparticles in MR imaging and drug delivery," *Advanced Drug Delivery Reviews*, vol. 60, no. 11, pp. 1252–1265, 2008.

[11] M. Levy, A. Quarta, A. Espinosa et al., "Correlating magneto-structural properties to hyperthermia performance of highly monodisperse iron oxide nanoparticles prepared by a seeded-growth route," *Chemistry of Materials*, vol. 23, no. 18, pp. 4170–4180, 2011.

[12] S.-H. Hu, B.-J. Liao, C.-S. Chiang, P.-J. Chen, I.-W. Chen, and S.-Y. Chen, "Core-shell nanocapsules stabilized by single-component polymer and nanoparticles for magneto-chemotherapy/hyperthermia with multiple drugs," *Advanced Materials*, vol. 24, no. 27, pp. 3627–3632, 2012.

[13] S. S. Lucky, K. C. Soo, and Y. Zhang, "Nanoparticles in photodynamic therapy," *Chemical Reviews*, vol. 115, no. 4, pp. 1990–2042, 2015.

[14] A. J. Cole, V. C. Yang, and A. E. David, "Cancer theranostics: the rise of targeted magnetic nanoparticles," *Trends in Biotechnology*, vol. 29, no. 7, pp. 323–332, 2011.

[15] E.-K. Lim, T. Kim, S. Paik, S. Haam, Y.-M. Huh, and K. Lee, "Nanomaterials for theranostics: recent advances and future challenges," *Chemical Reviews*, vol. 115, no. 1, pp. 327–394, 2015.

[16] L. Carbone and P. D. Cozzoli, "Colloidal heterostructured nanocrystals: synthesis and growth mechanisms," *Nano Today*, vol. 5, no. 5, pp. 449–493, 2010.

[17] M. Casavola, R. Buonsanti, G. Caputo, and P. D. Cozzoli, "Colloidal strategies for preparing oxide-based hybrid nanocrystals," *European Journal of Inorganic Chemistry*, no. 6, pp. 837–854, 2008.

[18] M. R. Buck, J. F. Bondi, and R. E. Schaak, "A total-synthesis framework for the construction of high-order colloidal hybrid nanoparticles," *Nature Chemistry*, vol. 4, no. 1, pp. 37–44, 2012.

[19] T. Pellegrino, A. Fiore, E. Carlino et al., "Heterodimers based on CoPt3-Au nanocrystals with tunable domain size," *Journal of the American Chemical Society*, vol. 128, no. 20, pp. 6690–6698, 2006.

[20] A. W. H. Lin, C. Yen Ang, P. K. Patra et al., "Seed-mediated synthesis, properties and application of γ-Fe_2O_3-CdSe magnetic quantum dots," *Journal of Solid State Chemistry*, vol. 184, no. 8, pp. 2150–2158, 2011.

[21] H. B. Na, G. Palui, J. T. Rosenberg, X. Ji, S. C. Grant, and H. Mattoussi, "Multidentate catechol-based polyethylene glycol oligomers provide enhanced stability and biocompatibility to iron oxide nanoparticles," *ACS Nano*, vol. 6, no. 1, pp. 389–399, 2012.

[22] G. Palui, T. Avellini, N. Zhan et al., "Photoinduced phase transfer of luminescent quantum dots to polar and aqueous media," *Journal of the American Chemical Society*, vol. 134, no. 39, pp. 16370–16378, 2012.

[23] H. R. Neves, R. A. Bini, J. H. O. Barbosa, C. E. G. Salmon, and L. C. Varanda, "Dextran-Coated Antiferromagnetic MnO Nanoparticles for a T_1-MRI Contrast Agent with High Colloidal Stability," *Particle and Particle Systems Characterization*, vol. 33, no. 3, pp. 167–176, 2016.

[24] W. Wu, Z. Wu, T. Yu, C. Jiang, and W.-S. Kim, "Recent progress on magnetic iron oxide nanoparticles: synthesis, surface functional strategies and biomedical applications," *Science and Technology of Advanced Materials*, vol. 16, no. 2, Article ID 023501, 2015.

[25] W. Wang, A. Kapur, X. Ji, B. Zeng, D. Mishra, and H. Mattoussi, "Multifunctional and high affinity polymer ligand that provides bio-orthogonal coating of quantum dots," *Bioconjugate Chemistry*, vol. 27, no. 9, pp. 2024–2036, 2016.

[26] S. T. Selvan, P. K. Patra, C. Y. Ang, and J. Y. Ying, "Synthesis of silica-coated semiconductor and magnetic quantum dots and their use in the imaging of live cells," *Angewandte Chemie—International Edition*, vol. 46, no. 14, pp. 2448–2452, 2007.

[27] C. G. S. Souza, W. Beck Jr., and L. C. Varanda, "Multifunctional luminomagnetic FePt@Fe_3O_4/SiO_2/Rhodamine B/SiO_2 nanoparticles with high magnetic emanation for biomedical applications," *Journal of Nanoparticle Research*, vol. 15, no. 4, 2013.

[28] T. C. Preston and R. Signorell, "Growth and optical properties of gold nanoshells prior to the formation of a continuous metallic layer," *ACS Nano*, vol. 3, no. 11, pp. 3696–3706, 2009.

[29] J. B. Blanco-Canosa, I. L. Medintz, D. Farrel, H. Mattoussi, and P. E. Dawson, "Rapid covalent ligation of fluorescent peptides to water solubilized quantum dots," *Journal of the American Chemical Society*, vol. 132, no. 29, pp. 10027–10033, 2010.

[30] N. Zhan, G. Palui, M. Safi, X. Ji, and H. Mattoussi, "Multidentate zwitterionic ligands provide compact and highly biocompatible quantum dots," *Journal of the American Chemical Society*, vol. 135, no. 37, pp. 13786–13795, 2013.

[31] S. Laurent, D. Forge, M. Port et al., "Magnetic iron oxide nanoparticles: synthesis, stabilization, vectorization, physicochemical characterizations, and biological applications," *Chemical Reviews*, vol. 108, pp. 2064–2110, 2008.

[32] J. Kim, H. S. Kim, N. Lee et al., "Multifunctional uniform nanoparticles composed of a magnetite nanocrystal core and a mesoporous silica shell for magnetic resonance and fluorescence imaging and for drug delivery," *Angewandte Chemie—International Edition*, vol. 47, no. 44, pp. 8438–8441, 2008.

[33] M. Vibin, R. Vinayakan, A. John et al., "Cytotoxicity and fluorescence studies of silica-coated CdSe quantum dots for bioimaging applications," *Journal of Nanoparticle Research*, vol. 13, no. 6, pp. 2587–2596, 2011.

[34] Y. Kobayashi, H. Katakami, E. Mine, D. Nagao, M. Konno, and L. M. Liz-Marzán, "Silica coating of silver nanoparticles using a modified Stöber method," *Journal of Colloid and Interface Science*, vol. 283, no. 2, pp. 392–396, 2005.

[35] L. C. Varanda, M. Imaizumi, F. J. Santos, and M. Jafelicci Jr., "Iron oxide versus $Fe_{55}Pt_{45}$/Fe_3O_4: improved magnetic properties of core/shell nanoparticles for biomedical applications," *IEEE Transactions on Magnetics*, vol. 44, no. 11, pp. 4448–4451, 2008.

[36] C. B. Murray, D. J. Norris, and M. G. Bawendi, " Synthesis and characterization of nearly monodisperse CdE (E = sulfur, selenium, tellurium) semiconductor nanocrystallites," *Journal of the American Chemical Society*, vol. 115, no. 19, pp. 8706–8715, 1993.

[37] L. C. Varanda and M. Jafelicci Jr., "Self-assembled FePt nanocrystals with large coercivity: Reduction of the fcc-to-$L1_0$ ordering temperature," *Journal of the American Chemical Society*, vol. 128, no. 34, pp. 11062–11066, 2006.

[38] W. Beck, C. G. Souza, T. L. Silva, M. Jafelicci, and L. C. Varanda, "Formation mechanism via a heterocoagulation approach of FePt nanoparticles using the modified polyol process," *The Journal of Physical Chemistry C*, vol. 115, no. 21, pp. 10475–10482, 2011.

[39] Y. J. Wong, L. Zhu, W. S. Teo et al., "Revisiting the Stöber method: Inhomogeneity in silica shells," *Journal of the American Chemical Society*, vol. 133, no. 30, pp. 11422–11425, 2011.

[40] J. I. Langford and A. J. C. Wilson, "Scherrer after 60 years—survey and some new results in determination of crystallite size," *Journal of Applied Crystallography*, vol. 11, no. APR, pp. 102–113, 1978.

[41] S. Sun, E. E. Fullerton, D. Weller, and C. B. Murray, "Compositionally controlled FePt nanoparticle materials," *IEEE Transactions on Magnetics*, vol. 37, no. 4, pp. 1239–1243, 2001.

[42] A. P. Alivisatos, "Semiconductor clusters, nanocrystals, and quantum dots," *Science*, vol. 271, no. 5251, pp. 933–937, 1996.

[43] D. J. Norris and M. G. Bawendi, "Measurement and assignment of the size-dependent optical spectrum in CdSe quantum dots," *Physical Review B*, vol. 53, no. 24, pp. 16338–16346, 1996.

[44] S. Bedanta and W. Kleemann, "Supermagnetism," *Journal of Physics D: Applied Physics*, vol. 42, no. 1, Article ID 013001, 2009.

[45] D. Segets, J. M. Lucas, R. N. Klupp Taylor et al., "Determination of the quantum dot band gap dependence on particle size from optical absorbance and transmission electron microscopy measurements," *ACS Nano*, vol. 6, no. 10, pp. 9021–9032, 2012.

[46] J. Jasieniak, L. Smith, J. Van Embden, P. Mulvaney, and M. Califano, "Re-examination of the size-dependent absorption properties of CdSe quantum dots," *Journal of Physical Chemistry C*, vol. 113, no. 45, pp. 19468–19474, 2009.

[47] R. Karel Čapek, I. Moreels, K. Lambert et al., "Optical properties of zincblende cadmium selenide quantum dots," *Journal of Physical Chemistry C*, vol. 114, no. 14, pp. 6371–6376, 2010.

[48] W. W. Yu, L. Qu, W. Guo, and X. Peng, "Experimental determination of the extinction coefficient of CdTe, CdSe and CdS nanocrystals," *Chemistry of Materials*, vol. 15, no. 14, pp. 2854–2860, 2004.